Available online at www.sciencedirect.com

ScienceDirect

Energy Procedia 48 (2014) 543 – 553

Energy Procedia

SHC 2013, International Conference on Solar Heating and Cooling for Buildings and Industry
September 23-25, 2013, Freiburg, Germany

Coloured solar-thermal absorbers – a comparative analysis of cermet structures

Anca Duta[a], Luminita Isac[a], Andrea Milea[a], Elena Ienei[a], Dana Perniu[a*]

[a]*RTD Center Renewable Energy Systems and Recycling, Transilvania University of Brasov, Eroilor 29, 500036 Brasov, Romania*

Abstract

Novel coloured solar-thermal absorber coatings are obtained as thin films of alumina infiltrated with pigment oxides (Fe_2O_3 and V_2O_5) and sulfides (CuS). The coatings are stepwise obtained in successive spray pyrolysis depositions, using inorganic precursors. The composite layers have good crystallinity degree and develop various morphologies, with very different matrix-pigment infiltration; the addition of gold nanoparticles differently influences the properties, depending on the interactions with the precursor species: it can strongly decrease the thermal emittance, when embedded in the layers structure (Fe_2O_3) or it can form large aggregates on the matrix (V_2O_5) without significant effect on the optical properties. Bright red spectral selective coatings, with spectral selectivity of 12 were obtained using Fe_2O_3 hematite pigments.

Selection and peer review by the scientific conference committee of SHC 2013 under responsibility of PSE AG

Keywords: Solar thermal collectors, spectral selective coatings, coloured absorber plate, spray pyrolisys deposition

1. Introduction

The share of energy consumption in buildings steadily increased in the past decades, being now higher than the values corresponding to the industrial and transportation sectors, [1]. More than half of this energy is used for heating, cooling and air conditioning, and the heating and domestic hot water needs are usually supplied by on-site

* Corresponding author. Tel.: +40-723-561-089; fax: +40-372-729-698.
E-mail address: d.perniu@unitbv.ro

1876-6102
Selection and peer review by the scientific conference committee of SHC 2013 under responsibility of PSE AG
doi:10.1016/j.egypro.2014.02.064

systems, heavily relying on fossil fuels. The constraints imposed by the mitigation of the traditional raw materials and the environmental burden imposed by the greenhouse gases emissions pointed the renewables as feasible candidates, able to provide solutions for the further development of sustainable communities.

Solar thermal systems using flat plate collectors are already recognised as market competitive heat sources, particularly for domestic hot water and plenty of research was devoted to this topic, starting with the '60s. The absorber plate represents the key component in a solar thermal flat plate collector, hosting the conversion (UV and VIS radiation to heat) and the convection (involving mainly the NIR radiation). Coatings with high VIS-absorptance (α) and low IR emittance (ε_T) are widely used, reaching standard values of the solar spectral selectivity ($S = \alpha/\varepsilon_T$) over 9. To reach these values, paints and coatings are deposited on a metal substrate (aluminium or copper); the absorber layer consists of a matrix (inorganic, polymeric) embedding nano- or micro-sized ceramics and metal nano-particles, for enhancing the spectral selectivity. Additionally, considering functionality, the optical performances and spectral selectivity requirements should be completed by corrosion resistance in the working environment (temperature, water vapors, saline aerosols), thus limiting the actual range of materials to highly stable ceramic oxides, sulfides or nitrides (usually with the metal in its highest oxidation state) and to corrosion resistant metal nano-particles (e.g. gold or silver are preferred and less copper). The resulting absorber plates are mainly black or with blue shades because of the thin TiO_2 anti-reflective coating with anti-corrosion properties. Many papers are reporting on highly efficient solar thermal flat plate collectors and several review papers provide accurate syntheses on the state of the art, [2,3].

When mounting state of the art collectors on terraces or in dedicated solar-thermal farms, the colour does not represent a particular problem but when targeting extensive urban integration, e.g. in solar - facades, the monotony of black or blue collectors represent a serious barrier in the architectural acceptance, [4].

There are two main approaches for getting coloured flat plate solar thermal collectors: by colouring the glazing (with a predictable loss in transmittance) or by colouring the absorber plate; both topics are highly investigated, as integrated solar-thermal systems in the built environment recently faced a new interest coming from the market.

Coloured absorber plates are already reported but their implementation is still limited because their performances are usually lower comparing to the commercial standard values. Two types of layers can yield colour: Thickness Insensitive Solar Selective (TISS) coatings, based on inorganic pigment infiltration and Thickness Sensitive Solar Selective (TSSS) coatings, also possible to use for colouring the glazing. The TISS coatings can be obtained by direct deposition of the coloured pigment (metal oxides as Fe_2O_3, Cr_2O_3, CoO_x) deposited directly on Al sheets, [5] or embedded in polymer matrixes, e.g. polyurethane as reported in the SOLAB project, [6]; the TSSS coatings are reported as a combination of multilayers with variable (high/low) refractive index, directly deposited on the metal plate, [7,8] or on a ceramic/cermet substrate.

Hybrid organic-inorganic structures were recently reported as TISS for solar facades, [9], along with spinel structures, [10] or hard coatings of metal/dielectric type, developed in multi-layered structures as Al/TiAlON/TiAlOxNy/TiAlN, [11, 12]. By tailoring the composition, the grain size and grain distribution inside the layer(s), various colors can be obtained with spectral selectivity values ranging from 3 up to 19.

The survey on urban acceptance for facades integration or other architectural objects, [4], showed that there is a need of 10 up to 20 different colors that could minimally satisfy the architects' and designers' demands, with the preferred chromatics centered on blue and red, and less on yellow and green. This is another reason why there still is plenty of open research running on developing colored absorber plates, competitive and cost-effective.

Many deposition techniques are reported for obtaining spectral selective absorber coatings: electroplating (the first method actually proposed, [13]), PVD [14], sputtering [15], etc. Spray pyrolysis deposition (SPD) is also reported for obtaining the matrix or the full black cermet coating, [16, 17] and this technique has the advantages of low complexity, good reproducibility and low cost.

This paper describes and comparatively analyses, for the first time to the best of our knowledge, novel coloured TISS layers, fully obtained by SPD, by embedding Fe_2O_3, V_2O_5 and CuS pigments in an alumina matrix. The effects of gold nano-particles and of the TiO_2 anti-reflective thin film on the optical properties of the layers are also reported. The results are promising and show that various red, green-yellow and dark green colours can be developed as absorber coatings with spectral selectivity up to 12.

2. Experimental

2.1. Thin layers deposition

Absorber coatings were developed with the following structure: Al/Al_2O_3/(Fe_2O_3, V_2O_5 or Cu_xS without/with AuNP)/TiO_2, based on successive optimisation steps, using the spectral selectivity as output property. Each step was separately performed, allowing the samples to cool down to room temperature, before starting the next deposition.

Step 1: Substrate conditioning. Sample A

- The commercial Al substrate (99,5% Beofon, thickness 0.7 mm) was degreased and ultra-sonnicated, than it was conditioned in alkaline solution (10-15 g/L NaOH, 30-50 g/L Na_2CO_3, 30-50 g/L Na_3PO_4).
- A thin Al_2O_3 seeding layer with controlled thickness and porosity is obtained by anodization, in nitiric acid solution (HNO_3:H_2O = 1:1) for 10 min at 3A, [18]. Samples of 2.5x2.5 cm were further used as substrates in the spray pyrolysis deposition of active layers.

Step 2: SPD deposition of the alumina matrix. Sample A/OA

- The Al_2O_3 layer was obtained by SPD from aqueous solution of 0.25 mol/L $AlCl_3 \cdot 6H_2O$ (extra pure, Scharlau Chemie) and acetyl acetone (99+%, Sigma-Aldrich) as additive; the Al_2O_3 was deposited on the preheated substrate at 400°C, by 30 spraying sequences, using air as carrier gas, at 1.5 bar.

Step 3: SPD infiltration of the coloured pigments;
Samples: A/OA/(Fe_2O_3 or V_2O_5 or CuS) and A/OA/(Fe_2O_3 or V_2O_5 or CuS) /Au

- Precursors: water – ethanol mixtures (1:1 vol), using:
  - Fe_2O_3 : 0.2 mol/L $FeCl_3 \cdot 6H_2O$ (extra pure, Scharlau Chemie),
  - V_2O_5: 0.03 mol/L NH_4VO_3 (reagent grade, Scharlau Chemie),
  - CuS: 0.3 mol/L $CuCl_2 \cdot 2H_2O$ (99%, Scharlau Chemie) and 0.9 mol/L thiourea (99%, Scharlau Chemie);
- Metal nano-particles: 10 nm Au nanoparticles (Au-NP, prepared as described in [19]) were dispersed in the pigment precursor solution to obtain concentrations of 3.5; 35; 350 μmol/L; the best spectral selectivity values were obtained for layers prepared using 35 μmol/L concentration, therefore these samples were further studied.
- Deposition conditions: depositions from precursors systems, with/without Au-NP used the optimized conditions:
  - Fe_2O_3: T = 400°C; carrier gas: air at 1.5 bar; no. of spraying sequences: 20.
  - V_2O_5: T = 400°C; carrier gas: air at 1.5 bar; no. of spraying sequences: 40.
  - CuS: T = 250°C; carrier gas: air at 1.5 bar; no. of spraying sequences: 15.

Step 4: SPD deposition of the anti-reflective layer. Samples: A/OA/(Fe_2O_3 or V_2O_5 or CuS) /Au/TiO_2

- Precursor system: Titaniumtetraisopropoxide, TTIP (99.99%, Sigma-Aldrich) and acetylacetone AcAc in ethanol solution (TTIP:AcAc:EtOH = 1:1.5:22.5 vol).
- Deposition conditions: T = 250°C; carrier gas: air at 1.5 bar; no. of deposition sequences: 10. The as obtained films were annealed at 500ºC for 1 hour.

2.2. Characterization

Using the Fourier Transform Infrared Spectroscopy (FTIR, Bruker Vertex 70) the IR spectra in transmittance and in reflectance modes were obtained in the range of 2500 - 16500 nm, to evaluate the thermal emittance (ε_T) of the stacked thin composite films. The thermal emittance was calculated using equation (1) [20], as the weighted fraction between the absorbed energy and the Planck blackbody energy (I_P) at certain wavelength (λ) and temperature (ambient temperature, in this work).

$$\varepsilon_T = \frac{\int_{2.5}^{16.5} I_p(\lambda)(1-R(\lambda))d\lambda}{\int_{2.5}^{16.5} I_p(\lambda)d(\lambda)} \quad (1)$$

The solar absorptance (α_s) was calculated using equation (2) [20], from the reflectance spectra (λ = 250-2500 nm, Perkin Elmer Lambda 950 UV-VIS-NIR spectrophotometer, equipped with integrating sphere to 150 mm).

$$\alpha_s = \frac{\int_{0.25}^{2.5} I_{sol}(\lambda)(1-R(\lambda))d\lambda}{\int_{0.25}^{2.5} I_{sol}(\lambda)d(\lambda)} \quad (2)$$

where: $R(\lambda)$ is the material's reflectance and I_{sol} is the solar irradiance (ISO 9854-1, 1992) with an air mass of 1.5.

The optical properties were correlated with the crystalline structure (XRD, Bruker D8 Discover) and with the surface composition (EDS, Thermo), roughness (AFM, Ntegra Spectra) and morphology (SEM 3500N, Hitachi).

3. Results and Discussions

3.1. Crystalline structure

The thin films and their assemblies have poly-crystalline structures as Fig. 1 shows. The overall crystallinity degree is estimated based on the Scherrer's formula and the average dimensions of the crystallites are presented in Table 1.

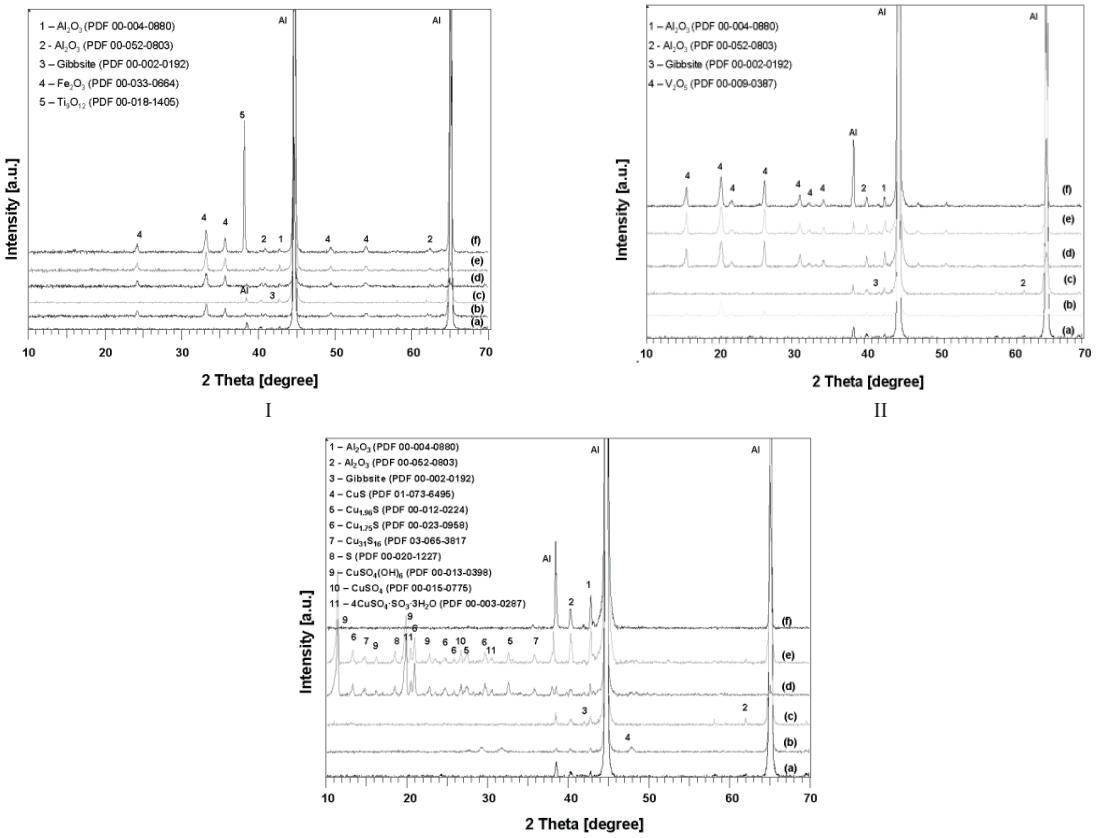

Fig. 1. XRD patterns of the thin films stepwise developed by infiltrating:
I. Fe_2O_3: (a) A; (b) A/Fe_2O_3; (c) A/AO; (d) A/AO/ Fe_2O_3; (e) A/AO/ Fe_2O_3/Au; (f) A/AO/ Fe_2O_3/Au/TiO_2
II. V_2O_5: (a) A; (b) A/V_2O_5; (c) A/AO; (d) A/AO/ V_2O_5; (e) A/AO/ V_2O_5/Au; (f) A/AO/ V_2O_5/Au/TiO_2
III. CuS: (a) A; (b) A/CuS; (c) A/AO; (d) A/AO/ CuS; (e) A/AO/ CuS/Au; (f) A/AO/ CuS/Au/TiO_2

In the early stages of the research, each layer was separately deposited on the pre-treated (A) substrate and the deposition parameters were optimized, considering the spectral selectivity. These layers (A/OA, A/Fe_2O_3, A/V_2O_5 and A/CuS) have, as outlined in Table 1, a high degree of crystallinity and a reduced number of polymorphs.

Table 1. Crystalline composition and crystallites sizes (D)

Sample	Crystalline Degree [%]	Crystalline structure and composition	D [nm]
A	93.3	Al_2O_3, cubic (17.67%); Al_2O_3, orthorhombic (82.33%)	50.61 (Al_2O_3)
A/OA	92.9	Al_2O_3, cubic (35.52%); Al_2O_3, orthorhombic (52.12%); Gibbsite, $Al_2O_3{\cdot}3H_2O$, monoclinic (12.36%)	31.49 (Al_2O_3)
A/ Fe_2O_3	87.9	Al_2O_3, cubic (1.7%); Al_2O_3, orthorhombic (2.58%); Hematite, syn, Fe_2O_3, rhombohedric (95.72%)	31.21 (Fe_2O_3)
A/OA/ Fe_2O_3	81.2	Al_2O_3, cubic (0.38%); Al_2O_3, orthorhombic (11.78%); Gibbsite, $Al_2O_3{\cdot}3H_2O$, monoclinic (1.68%); Hematite, syn, Fe_2O_3, rhombohedric (86.15%)	25.97 (Fe_2O_3)
A/OA/ Fe_2O_3/Au	91.5	Al_2O_3, cubic (5.09%); Hematite, syn, Fe_2O_3, rhombohedric (94.91%)	31.12 (Fe_2O_3)
A/OA/ Fe_2O_3/Au /TiO_2	92.9	Al_2O_3, cubic (1%); Hematite, syn, Fe_2O_3, rhombohedric (45.96%); Titanium oxide, Ti_9O_{12}, triclinic (53.04%)	30.28 (Fe_2O_3)
A/ V_2O_5	89.8	Al_2O_3, cubic (4.24%); Al_2O_3, orthorhombic (7.42%); Shcherbinaite, syn, V_2O_5, orthorhombic (88.34%)	23.84 (V_2O_5)
A/AO/ V_2O_5	93.6	Al_2O_3, cubic (6.75%); Al_2O_3, orthorhombic (5.56%); Gibbsite, $Al_2O_3{\cdot}3H_2O$, monoclinic (0.93%); Shcherbinaite, syn, V_2O_5, orthorhombic (86.75%)	21.38 (V_2O_5)
A/AO/ V_2O_5/Au	92.1	Al_2O_3, cubic (7.21%); Al_2O_3, orthorhombic (10.51%); Shcherbinaite, syn, V_2O_5, orthorhombic (82.27%)	20.51 (V_2O_5)
A/AO/ V_2O_5/Au /TiO_2	92.6	Al_2O_3, cubic (3.5%); Al_2O_3, orthorhombic (34.57%); Shcherbinaite, syn, V_2O_5, orthorhombic (61.93%)	23.08 (V_2O_5)
A/CuS	92	Al_2O_3, cubic (6.3%); Al_2O_3, orthorhombic (10.5%); Covellite, CuS, hexagonal (83.2%)	20.39 (CuS)
A/OA/CuS	89	Al_2O_3, cubic (1.88%); Sulfur, S (21.82%); Copper sulphate hydrate, $4CuO{\cdot}SO_3{\cdot}3H_2O$ (1.83%); Brochantite-O, $CuSO_4(OH)_6$. monoclinic (35.54%); Chalcocyanite, syn, $CuSO_4$, orthorhombic (1.36%); Covellite, CuS, hexagonal (1.02%); Copper sulfide, $Cu_{1.96}S$, tetragonal (6.83%); Roxybite, syn, Cu_7S_4, monoclinic (24.38%); Djurleite, $Cu_{31}S_{16}$, monoclinic (5.34%)	-
A/OA/CuS /Au	95.1	Al_2O_3, cubic (0.86%); Sulfur, S (19.07%); Copper sulphate hydrate, $4CuO{\cdot}SO_3{\cdot}3H_2O$ (2.19%); Brochantite-O, $CuSO_4(OH)_6$. monoclinic (34.33%); Chalcocyanite, syn, $CuSO_4$, orthorhombic (2.34%); Copper sulfide, $Cu_{1.96}S$, tetragonal (6.83%); Roxybite, syn, Cu_7S_4, monoclinic (29.2%); Djurleite, $Cu_{31}S_{16}$, monoclinic (5.08%)	-
A/OA/CuS /Au /TiO_2	96.7	Al_2O_3, cubic (52.84%); Al_2O_3, orthorhombic (47.17%)	35.77 (Al_2O_3)

When developing the stacked layers in the absorber plate, by infiltrating the A/OA matrix, the crystallinity degree of the pigments is slightly decreased and a significant increase in polymorphism is registered for the CuS, along with the development of various other compounds of Cu, S and O. These results well match previous experiments that show that CuS can be obtained by SPD along with other non-stoichiometric compounds (Cu_xS, x=1.8-2), [21,22]; the results also show the influence of the alumina matrix on the composition of the CuS based absorber layers. It was already reported [23] that CuS thermal decomposition is a four-step process and, depending on the experimental conditions (temperature, atmosphere), different copper compounds may result: sulfides, oxides, sulfates, oxysulfates. The last two types of compounds are obtained at temperatures higher than 310^{o}C. The alumina

matrix may have a catalytic effect in the CuS thermal oxidation, forming copper sulfates and oxysulfates at the deposition temperature (T=250°C), which is lower than the values mentioned by literature. Different crystal growth is also observed when Au-NPs are inserted in the oxides precursor system, as result of different nucleation and growth on the alumina matrix (OA) and on the gold nanoparticles. The crystallite sizes of Fe_2O_3 and V_2O_5 grown on the Al/AlO film have an opposite variation in size when gold is added (increasing for iron and decreasing for vanadium oxide), thus one may conclude that the interactions between the precursors are different with gold: much stronger interaction of the hydrated iron ion (thus much slower nucleation) compared to the lower affinity of the VO_3^- anion. This leads to the conclusion that tailoring the surface charge of the matrix (OA is slightly negatively charged) and of the Au-NP may represent a tuning instrument of the poly-crystallinity in the films.

The addition of the anti-reflective layer of TiO_2 significantly affects the composites containing CuS; the EDS results still show copper and sulfur in the composition but, according to the XRD data, these compounds are no longer crystalline. On the more temperature-stable pigments, the effect of a supplementary deposition at temperatures close to their own deposition temperature has as effect a possible densification and increase in the crystallite size (as for V_2O_5) or the release of by-products, with slight crystallites shrinking (as for Fe_2O_3).

3.2. Elemental composition and surface homogeneity

The uniformity in the surface composition represents an important aspect, both for a good overall spectral selectivity and for reaching high stability and corrosion/erosion resistance. Therefore, Electron Dispersive Spectroscopy (EDS) was performed on the samples outlining the elemental composition and the variation limits on the 50 μm scanned lines, Table 2.

Table 2 Elemental composition of the thin layers

Sample	Elemental weight composition [%]							
	Al	O	Fe	V	Cu	S	Au	Ti
A	70 – 74	26 – 30						
A/OA	68 – 69	31 – 32						
A/Fe_2O_3	37 – 38	33 – 34.5	27 – 29					
A/OA/ Fe_2O_3	40 – 47	34 – 37	16.5 -20					
A/OA/ Fe_2O_3/Au	37.5 – 40	32 – 33	27 – 28				0 – 1.7	
A/OA/ Fe_2O_3/Au/TiO_2	24.5 – 31	32 – 33	30 – 37					5.6 – 7.5
A/V_2O_5	49 – 62	16 – 38		20 – 22				
A/AO/V_2O_5	55 – 66	22 – 33		11 – 12				
A/AO/ V_2O_5/Au	36 – 50	36 – 45		18 – 28			0.15 – 1	
A/AO/ V_2O_5/Au/ TiO_2	33 – 44	30 – 42.5		17 – 18				7.6 – 8.2
A/CuS	62 – 63	28 – 29			5.5 – 6	3 – 3.5		
A/OA/CuS	28 – 37	15 – 21			18 – 23	28 – 31		
A/OA/CuS /Au	25 – 42	17.5 – 31			18 – 21	26 – 35		
A/OA/CuS /Au/ TiO_2	28 –29.5	34 – 36			25 – 28	3.2– 3.8		3.6 – 7

The elemental composition analyzed by EDS gives information on the surface homogeneity and consequently on the growth and adherence of each layer on the previous one. As expected, the SPD deposition on the anodized

aluminum substrate closely respects the alumina composition and shows an increase in the oxygen content. Similar growth is registered also for Fe_2O_3 and CuS on the anodized aluminum foil but this is hardly the case for the vanadium oxide with an EDS composition that indicates that more oxygen:vanadium compounds could be present on the surface. Since the diffraction data showed only crystalline V_2O_5 one may conclude that the other possible compounds are amorphous. The deposition of the pigment layers on the thicker alumina matrix leads to rather good coverage (strongly improved for vanadium oxide) but the large variations in the Al content may outline that the pigment coating has different thicknesses. The Au-NPs addition has a different effect for iron and vanadium oxide, confirming that different interactions are governing the growth of these two layers. In all cases, the very low content of Au-NPs has as effect a very weak EDS signal, sometimes not traceable as for the CuS containing layers. On the other hand, the TiO_2 coverage is almost the same for all the samples, proving the versatility of this material.

3.3. Surface morphology

The data so far presented indicate possible large differences in the surface morphology and these are important factors in controlling the optical parameters. The SEM data of the samples developed for optimizing the deposition parameters are presented in Fig. 2.

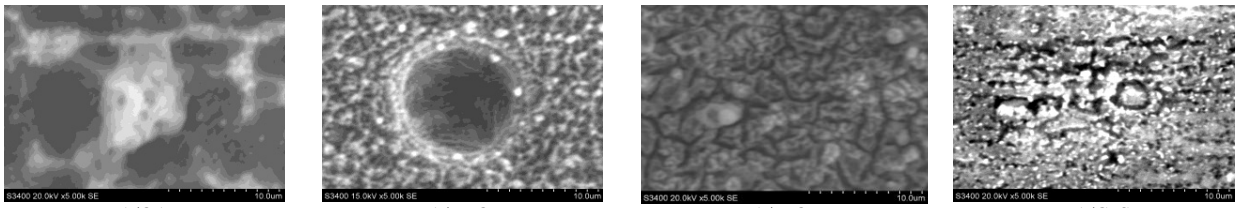

A/OA A/Fe_2O_3 A/V_2O_5 A/CuS

Fig. 2 SEM micrographs of the layers, component of the spectral selective composite

The highly porous alumina (A/OA) represents a good host for further infiltration with pigment layers. On the other hand, the pigment layers directly deposited on anodized Al have different morpholgies, ranging from macro-porous (A/Fe_2O_3) to dense layers, and are composed of larger associates sepparated by cracks. The optical properties are the consequence of materials' type and morphology, the latest contributing with multiple reflections and multiple scattering; the optimised morphologies in Fig. 2 are well supporting these processes.

Further SEM investigations are done on the absorber composite layers, Fig. 3 and are presented along with the average roughness values, as obtained from AFM images.

The results show a very good infiltration of the Fe_2O_3, particularly when Au-Np are included in the system. On the other hand, V_2O_5 homogenous infiltration is deficitar, actualy large agglomerates are formed on the alumina matrix (as A/OA/V_2O_5 shows) and/or grow on the Au-NPs. This preferential growth on the gold nano-particles is exhibited also by CuS. The TiO_2 layer seems to improve the aggregation in the CuS – containing composites but this effect is not enough for the V_2O_5 layer.

The average roughness is high for the composites containing Fe_2O_3 and the good infiltration during each step is confirmed by the almost constant values, slightly higher than the values corresponding to the alumina matrix (324 nm). The other two types of layers have an increasingly higher roughness following the deposition steps, confirming the irregular coverage that is increased by successive depositions.

To confirm these assumptions the AFM pictures of the samples with and without Au-NP addition were further analyzed and the results are presented in Fig. 4. These results show that the layers containing Fe_2O_3 accommodate the small gold NP among the columnar oxide structures while the CuS structure hardly can retain them, similarly to the flat V_2O_5 surface. The significant differences in the surface aspect of this latest sample confirm the EDS data, outlining the importance of the precursor type and charge when interacting with the metal nanoparticles.

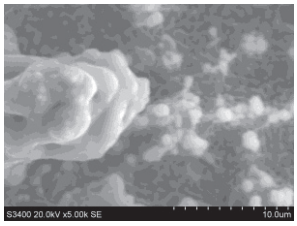
A/OA/Fe_2O_3
Sa = 446 nm

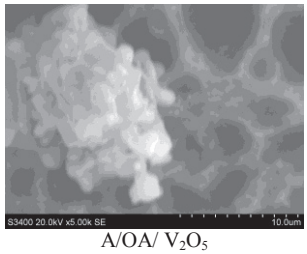
A/OA/ V_2O_5
Sa = 96 nm

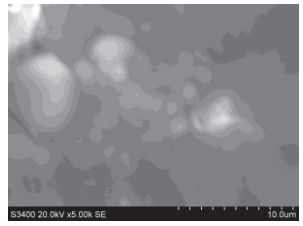
A/OA/CuS
Sa = 50 nm

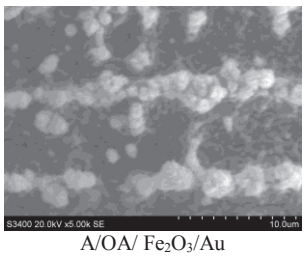
A/OA/ Fe_2O_3/Au
Sa = 438 nm

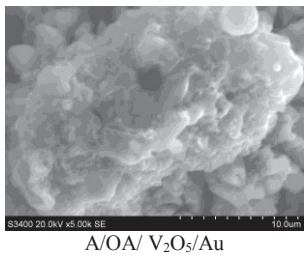
A/OA/ V_2O_5/Au
Sa = 55 nm

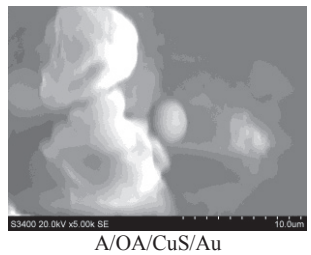
A/OA/CuS/Au
Sa = 152 nm

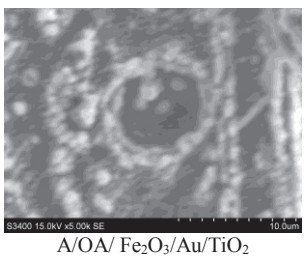
A/OA/ Fe_2O_3/Au/TiO_2
Sa = 451 nm

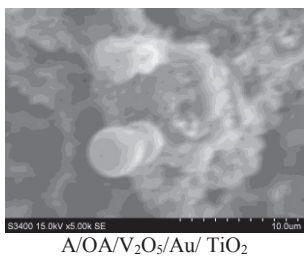
A/OA/V_2O_5/Au/ TiO_2
Sa = 216 nm

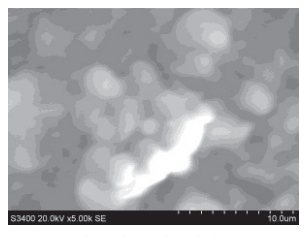
A/OA/CuS/Au/TiO_2
Sa = 327 nm

Fig. 3 SEM micrographs and average roughness (AFM) of the composite layers

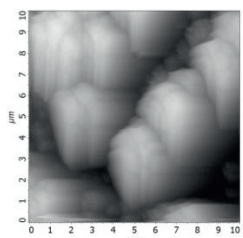
A/OA/Fe_2O_3
Surface Skewness: - 0.142

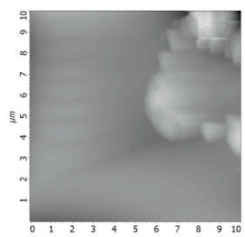
A/OA/V_2O_5
Surface Skewness: + 0.710

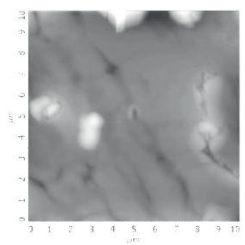
A/OA/CuS
Surface Skewness: + 0.142

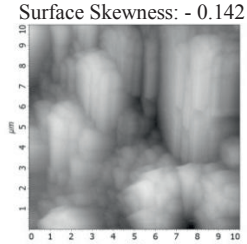
A/OA/Fe_2O_3/Au
Surface Skewness: - 0.662

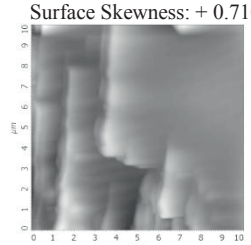
A/OA/V_2O_5/Au
Surfacekewness: + 0.840

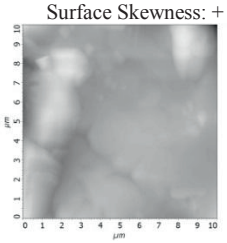
A/OA/CuS/Au
Surface Skewness: + 0.285

Fig. 4. AFM images and surface skewness of the spectral selective layers

It is also important to notice the negative surface skewness of the layers containing Fe_2O_3, similar to the A/OA substrate (Surface Skewness = - 0.362), confirming almost homogeneous infiltration in the surface voids as result of a uniform nucleation, consequence of interaction between the alumina matrix and the iron cation precursor. The same could be expected for CuS but the thioureea complexes (due to thioureea large excess) may distore the copper cation/matrix interaction through temporar adsorption, generating surface peaks (positive values of the surface skewness).

3.4. Optical properties and spectral selectivity

The optical properties, presented in Table 3 can now be explained, based on the above results. Performant (and black) spectral selective coatings have state of the art solar absorptance values (α_{sol}) above 0.9 and thermal emittance (ε_T) bellow 0.1. As expected, the solar absorptance is lower for the light coloured composites, although the dark green CuS thin films have encouraging values. The thermal emittance is expected to decrease when embbeding metal nanoparticles but this effect is signficant only for the structures containing Fe_2O_3. For partially incorporated particles (in structures containing CuS) the effect is less obvious and it is completely lost when the metal oxides covers the NPs but are not infiltrating the matrix, as the V_2O_5 case is.

Table 3 optical properties and spectral selectivity of the composite layers

Sample	α_{sol}	ε_T	S
A	0.32	0.18	1.78
A/AO	0.29	0.14	2.07
A/Fe_2O_3	0.54	0.16	3.38
A/AO/ Fe_2O_3	0.63	0.15	4.20
A/AO/ Fe_2O_3/Au	**0.62**	**0.05**	**12.40**
A/AO/ Fe_2O_3/Au / TiO_2	**0.65**	**0.07**	**9.29**
A/V_2O_5	0.55	0.23	2.39
A/AO/ V_2O_5	0.41	0.12	3.42
A/AO/ V_2O_5/Au	0.52	0.17	3.06
A/AO/ V_2O_5/Au/ TiO_2	0.53	0.14	3.79
A/CuS	0.95	0.36	2.64
A/AO/CuS	0.79	0.58	1.36
A/AO/CuS /Au	0.75	0.23	3.26
A/AO/CuS /Au /TiO_2	0.69	0.20	3.45

Corroborating these results with the morphology data one may conclude that only well infiltrated composites, with porous surface, forming true cermets are successful candidates for solar –thermal performant absorber coatings. The best result, market competitive, is obtained for the A/AO/Fe_2O_3/Au structure, and adding a protective TiO_2 layer still preserves this layer competitiveness. Further investigations on the durability of the coatings and benchmarking the results will be performed, as a compulsory step for scaling up.

4. Conclusions

Spectral selective coatings for absorbers in solar thermal flat plate collectors with high architectural acceptance were obtained as composite structures of coloured pigments embbeded in alumina matrix. Three types of structures were analysed, having Fe_2O_3, V_2O_5 and CuS as red, green-yellow and dark green pigments. The results show that the most important aspect in getting competitive spectral selectivity is the good and uniform reciprocal infiltration of the composites‘ layers, and this is obtained when good interfaces are developed between the layers, for structures with extended crystallinity and high roughness (composites containing Fe_2O_3). By adding gold nanoparticles, depending on the precursor type, the growth is uniform – embedding the NP in the layer, or preferentially runs on the NP, as for V_2O_5; thus, adequately matching the Au-NPs surface charge with that of the precursor represents a path for optimizing the composite structure, towards enhanced spectral selectivity. The composites were fully obtained by spray pyrolysis depositions, proving that this technique is competitive and well supports scaling up.

Acknowledgements

This paper is supported by the projects EST IN URBA 28/2012 and NANOVISMAT 162/2012, PN-II-PT-PCCA-2011-3.2-1235, developed within the program PNII – Partnership in priority domain, with the support of ANCS, CNDI-UEFISCDI.

References

[1] Pérez-Lombard L, Ortiz J, Pout C. A review on buildings energy consumption information. Energ. Buildings, 2008; 40: 394-8.
[2] Kalogirou SA. Solar thermal collectors and applications. Prog. Energ. Combust. 2004; 30: 231–95.
[3] Wijewardane S, Goswami DY. A review on surface control of thermal radiation by paints and coatings for new energy applications. Ren. Sust. Energ. Rev. 2012; 16: 1863–73.
[4] Munari Probst MC, Roecker C. Towards an improved architectural quality of building integrated solar thermal systems (BIST). Sol. Energy. 2007; 81 1104–16.
[5] Crnjak OZ, Klanjzsek GM, Hutchins MG. Spectrally selective solar absorbers in different non-black colours. Sol.Energ.Mat. Sol C.. 2005; 85: 41–50.
[6] Orel B, Spreizer H, Vuk AS, Fir M, Merlini D, Vodlan M, Kohl M. Selective paint coatings for colored solar absorbers: polyurethane thickness insensitive spectrally selective (TISS) paints (part II). Sol.Energ.Mat. Sol C., 2007; 91:108–19.
[7] Schuler A, Boudaden J, Oelhafen P, De Chambrier E, Roecker C, Scartezzini J-L. Thin film multilayer design types for colored glazed thermal solar collectors. Sol.Energ.Mat. Sol C.. 2005; 89 219–31.
[8] Etherden N, Tesfamichael T, Niklasson GA, Wackelgard E. A theoretical feasibility study of pigments for thickness-sensitive spectrally selective paints. J. Phys D: Appl. Phys. 2004; 37:1115–22.
[9] Quesada G, Rousse D, Dutil Y, Badache M, Hallé S. A comprehensive review of solar facades. Opaque solar facades, Ren Sust Energ Rev. 2012; 16: 2820–32.
[10] Geng Q, Zhao X, Gao X, Yu H, Yang S, Liu G. Optimization design of CuCrxMn2−xO4-based paint coatings used for solar selective applications. Sol.Energ.Mat. Sol C.. 2012; 105: 293–301.
[11] Zhao S, Chromaticity and optical properties of colored and black solar–thermal absorbing coatings. Sol.Energ.Mat. Sol C. 2010; 94: 1630–5.
[12] Mao F, Zhao S. The influence of oxygen in TiAlOxNy on the optical properties of colored solar-absorbing coatings. Sol.Energ.Mat. Sol C.. 2012; 98: 179–84.
[13] Hutchins MG. Spectrally selective solar absorber coatings. Appl. Energ. 1979; 5: 251–62.
[14] Selvakumar N, Barshilia HC. Review of physical vapor deposited (PVD), spectrally selective coatings for mid- and high-temperature solar thermal applications. Sol.Energ.Mat. Sol C.. 2012; 98: 1–23.
[15] Zheng L, Gao F, Zhao S, Zhou F, Nshimiyimana JP, Diao X. Optical design and co-sputtering preparation of high performance Mo–SiO2 cermet solar selective absorbing coatin. Appl. Surf. Sci. 2013; 280: 240–6.
[16] Ienei E, Isac L, Cazan C, Duta A. Characterization of Al/Al(2)O(3)/NiO(x) solar absorber obtained by spray pyrolysis. Solid State Sci. 2010; 12:1894-7.
[17] Chidambaram K, Malhotra LK, Chopra KL. Spray-pyrolysis cobalt black as a high temperature selective absorber. Thin Solid Films 1982; 87:365–71.
[18] Anicai L, Trifu C, Dima L. Anodic oxidation and coloring of aluminum powders. Metal Finishing. 2000; 98:20-25.
[19] Mihaly M, Fleancu MC, Olteanu NL, Bojin D, Meghea A, Enachescu M. Synthesis of gold nanoparticles by microemulsion assisted photoreduction method. Comptes Rendus Chimie. 2012; 15: 1012–21.
[20] Ienei E, Isac L, Duta A. Synthesis of alumina thin films by spray pyrolysis. Rev. Roum. Chim. 2010; 55: 161-5.
[21] Isac L, Popovici I, Enesca A, Duta A, Thin films as possible p-type absorbers in 3D solar cells, Energy Procedia. 2010: 2: 71-8.

[22] Isac L, Andronic L, Enesca A, Duta A, Copper sulfide films obtained by spray pyrolysis for dyes photodegradation under visible light irradiation. J. Photoch. Photobio A: Chemistry. 2013; 252: 53–9.
[23] Simionescu CM, Teodorescu VS, Carp O, Patron L, Thermal behaviour of CuS (covellite) obtained from copper-thiosulfate system, Journal of Therm. Anal. Calorim. 2007: 88: 71-6.